JGR Space Physics

RESEARCH ARTICLE
10.1029/2020JA028596

Hints on the Multiscale Nature of Geomagnetic Field Fluctuations During Quiet and Disturbed Periods

L. Santarelli[1,2], **P. De Michelis**[3], **and G. Consolini**[4]

[1]Istituto Nazionale di Geofisica e Vulcanologia, L'Aquila, Italy, [2]Università degli Studi dell'Aquila, L'Aquila, Italy, [3]Istituto Nazionale di Geofisica e Vulcanologia, Rome, Italy, [4]INAF-Istituto di Astrofisica e Planetologia Spaziali, Rome, Italy

Key Points:

- The multiscale nature of geomagnetic field fluctuations recorded on the ground is analyzed
- Short-timescale magnetic fluctuations constitute a significant contribution to the magnetic field of external origin at high latitudes
- The main source of short timescale magnetic fluctuations seems to be the occurrence of magnetospheric substorms

Correspondence to:
P. De Michelis,
paola.demichelis@ingv.it

Citation:
Santarelli, L., De Michelis, P., & Consolini, G. (2021). Hints on the multiscale nature of geomagnetic field fluctuations during quiet and disturbed periods. *Journal of Geophysical Research: Space Physics*, *126*, e2020JA028596. https://doi.org/10.1029/2020JA028596

Received 18 AUG 2020
Accepted 19 APR 2021

Abstract We analyze the geomagnetic data recorded at 78 stations from 13 to 31 March 2015. Using the empirical mode decomposition (EMD) method, we focus our attention on geomagnetic signal due to sources which are external to the Earth, that is, due to current systems flowing in the ionosphere and magnetosphere. We analyze the short timescale fluctuations ($\tau < 200$ min) of this magnetic signal, their dependence on magnetic latitude, magnetic local time, and geomagnetic activity. At high geomagnetic latitudes (>|60°|), these short timescale fluctuations constitute more than 30% of the external magnetic field. Their maximum contribution occurs along the auroral oval suggesting that they are mainly triggered by the ionospheric electric current systems active in these regions. A discussion of the relevance of these short timescale magnetic fluctuations to result in a more significant modeling and prediction of geomagnetically induced currents in the auroral zones is also provided.

1. Introduction

Since the beginning of the 90s it has been understood that during the geomagnetically disturbed periods and more exactly during the occurrence of geomagnetic storms and magnetospheric substorms, the Earth's magnetosphere does not respond passively to the solar wind and interplanetary medium changes but, conversely, it shows a very rich dynamic, characterized by non-linear processes (Ahn et al., 1983; Tsurutani et al., 1990; Vassiliadis et al., 1990). Various studies, conducted using both different methodologies and datasets, have highlighted some specific features of the magnetospheric dynamics, such as the non-linearity, bursty-activity and scale invariance which have allowed to hypothesize that the magnetosphere may be considered as an open system in an out-of-equilibrium configuration near criticality (Consolini, 1997, 2002; Consolini et al., 2008; Sharma, 2001; Sitnov et al., 2000, 2001; Uritsky et al., 2002; Uritsky & Pudovkin, 1998).

Considering the magnetosphere as a complex system out-of-equilibrium, this, like many complex systems, when continuously driven tends to a state showing self-organization and a non-trivial dynamics characterized by cooperativity and multiscale features. It is the reason why the magnetosphere shows macroscopic properties, including collective behaviors, which are coherent on large scales. However, although on a large spatial scale the dynamics of the magnetosphere recalls that of a low-dimensional dynamic system and therefore of a system characterized by a few degrees of freedom, at smaller spatial and temporal scales the magnetospheric dynamics is more complex, presenting a multiscale behavior. This means that a large number of spatial and temporal scales can be involved in the magnetospheric dynamics. Therefore, a key feature of the magnetospheric dynamics is the coexistence of global coherence and multiscale behavior.

Focusing on the multiscale behavior of the magnetospheric dynamics we notice that the nonlinear processes occurring over a wide range of spatial and temporal scales can be directly driven by the solar wind or can be the result of dynamical processes taking place in the magnetosphere, which are obviously triggered by changes in the solar wind and in the interplanetary magnetic field orientation. This means that the nonlinear processes on the basis of the magnetospheric dynamics although triggered by the variation of the interplanetary conditions, can be also strongly affected by magnetospheric internal conditions.

Recently, investigating the behavior of some geomagnetic indices (AE indices, SYM-H and ASY-H), the Perreault-Akasofu coupling function and the Bz component of the interplanetary magnetic field, it has been displayed (Alberti et al., 2017) that the magnetic time series, associated with the geomagnetic indices, are characterized by fluctuations which present a different amount of shared information (which

is representative of a different correlation degree) with the interplanetary magnetic field and solar wind parameters according to the analyzed timescale. The different amount of shared information between the magnetic fluctuations, both on short and on long timescales, and the interplanetary magnetic field and solar wind parameters has been interpreted in terms of a different origin of the magnetospheric dynamics at the different timescales. It has been suggested that there exists a "fast" magnetospheric dynamics which is described by fluctuations occurring on short timescales, and a "slow" magnetospheric dynamics which is well described by fluctuations on long timescales. The fast magnetospheric dynamics seems to be mainly influenced by the internal state of the magnetosphere while the slow magnetospheric dynamics, although related to the state and processes taking place within the magnetosphere, seems to be more directly driven by the solar wind changes. The threshold between these two different timescales has been identified around 200 min (Alberti et al., 2017). This value is well in agreement with the timescale found by Tsurutani et al. (1990) where a clear separation between the linear and nonlinear response of the magnetosphere to the external forcing of the solar wind was found at around this value. Hence, the terminology of fast and slow dynamics refers to the timescale separation of the fluctuations which are more or less (linearly or non-linearly) directly linked to changes in the solar wind, that is, more or less influenced by a dynamics directly driven by sources external to the magnetosphere or by a dynamics internal to it. This means that the slow and fast dynamics refer to the dynamics of fluctuations at different timescales and do not refer to the typical timescales of the magnetospheric response, which can be of the order of several tens of minutes (Baker et al., 1995; Bargatze et al., 1985).

The aim of this work is to study the nature and character of the Earth's magnetic field fluctuations recorded on the ground during a magnetically disturbed period. The idea is to investigate the properties of the Earth's magnetic field fluctuations associated with the different timescales, paying attention to the characterization of the multiscale nature of these fluctuations, that is, the simultaneous involvement of the fluctuations over a wide range of timescales. The identification of timescales directly connected to the external variability of the solar wind and to the internal magnetospheric dynamics is important for Space Weather studies; a correct characterization of the slow and fast dynamics and of the processes at their origin represent a key point for this kind of studies. In fact, understanding the phenomena occurring at different timescales is of fundamental importance to correctly forecast the magnetospheric dynamics. Some attempts to predict geomagnetic activity in terms of geomagnetic indices have clearly shown the difficulty of reproducing the dynamics on short timescales (typically below one hour) using only the interplanetary magnetic field and solar wind plasma parameters (see for example Pallocchia et al., 2007). This is an important point in the Space Weather especially considering that there are processes, such as the generation of geomagnetically induced currents, that depend on the intensity and speed of the magnetic field fluctuations recorded on the ground. Therefore, the ability to correctly forecast magnetic field fluctuations on short timescales is a starting point for an accurate forecast and subsequent mitigation of some relevant processes taking place on the ground due to Space Weather events.

In this work we try to answer to some interesting questions: Can the magnetic field measurements recorded on the ground help us to understand the magnetospheric dynamics in response to changes in the solar wind and the interplanetary magnetic field conditions? Can we identify in the magnetic signal the contribution directly connected to the external variability of the solar wind and that mainly due to the internal magnetospheric dynamics? In a magnetic signal, is the relationship between these two different contributions constant or is a function of latitude and geomagnetic activity?

2. Data

We examine the geomagnetic field fluctuations recorded on the ground during a period of 19 days: from 13 to 31 March 2015. This period is characterized by different levels of geomagnetic activity as it is shown by the temporal trends of two geomagnetic indices, AE (Davis & Sugiura, 1966) and SYM-H (Iyemori & Rao, 1996) reported in Figure 1. These two geomagnetic indices, which have 1 min time resolution, provide a good description of the magnetic effects on the ground due to ionospheric and magnetospheric current systems flowing at high- and low/mid-latitude regions. The values assumed by these two indices in the selected period reveal the existence of days characterized by a low level of geomagnetic activity (from 13 to 16 March 2015), days characterized by a high level of geomagnetic disturbance (from 17 to 19 March 2015)

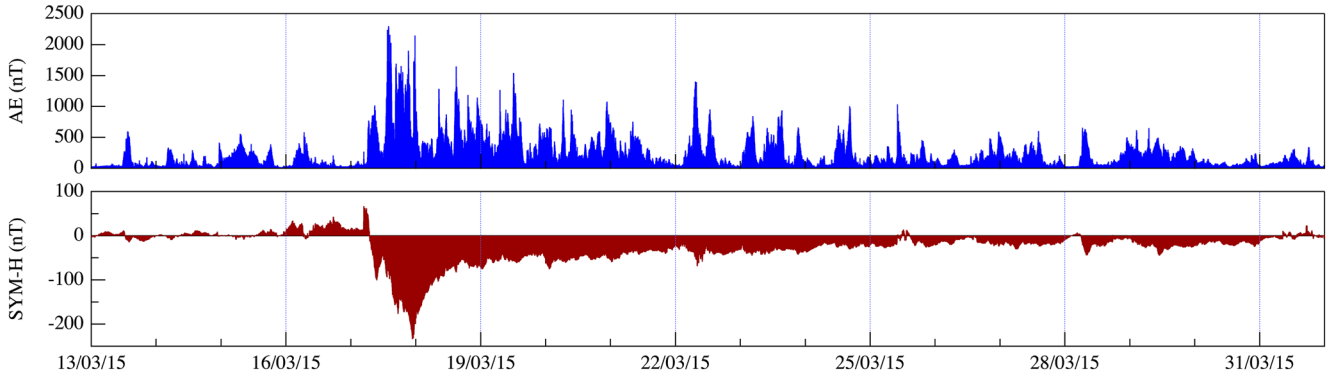

Figure 1. Temporal trends of AE and SYM–H indices between 13 and 31 March 2015.

and days with a moderate geomagnetic activity (from 20 to 23 March 2015). The selected period includes the famous magnetic storm of March 17, 2015, known as St. Patrick's Day storm, on which we will pay particular attention in our analysis.

We consider the geographic North (X) and geographic East (Y) components of the Earth's magnetic field in the geodetic reference frame with a temporal resolution of 1 min recorded by magnetometers placed both at permanent observatories and magnetometer stations. This means that we consider the geomagnetic field components describing both the absolute level and the time-varying magnetic field in the case of data recorded at permanent observatories, and magnetic field components containing only the time-varying part of the Earth's magnetic field without its baseline in the case of data recorded at magnetometer stations. We use 78 stations located in the Northern and Southern hemispheres. The distribution of the selected stations is uneven and that is a well-known problem occurring when magnetic data recorded on the ground are used. Indeed, the magnetic stations network has considerable geographical gaps, which are mainly located in the Southern hemisphere and in the oceanic regions. For this reason, we select only a part of all magnetic stations located in Europe and North America trying to no emphasize the uneven distribution of the stations in the different parts of the world. Figure 2 shows the distribution of the selected stations and in Appendix A we report for each of them some information such as the International Association of Geomagnetism and Aeronomy (IAGA) identification code, the geographical and Quasi-Dipole (QD) magnetic

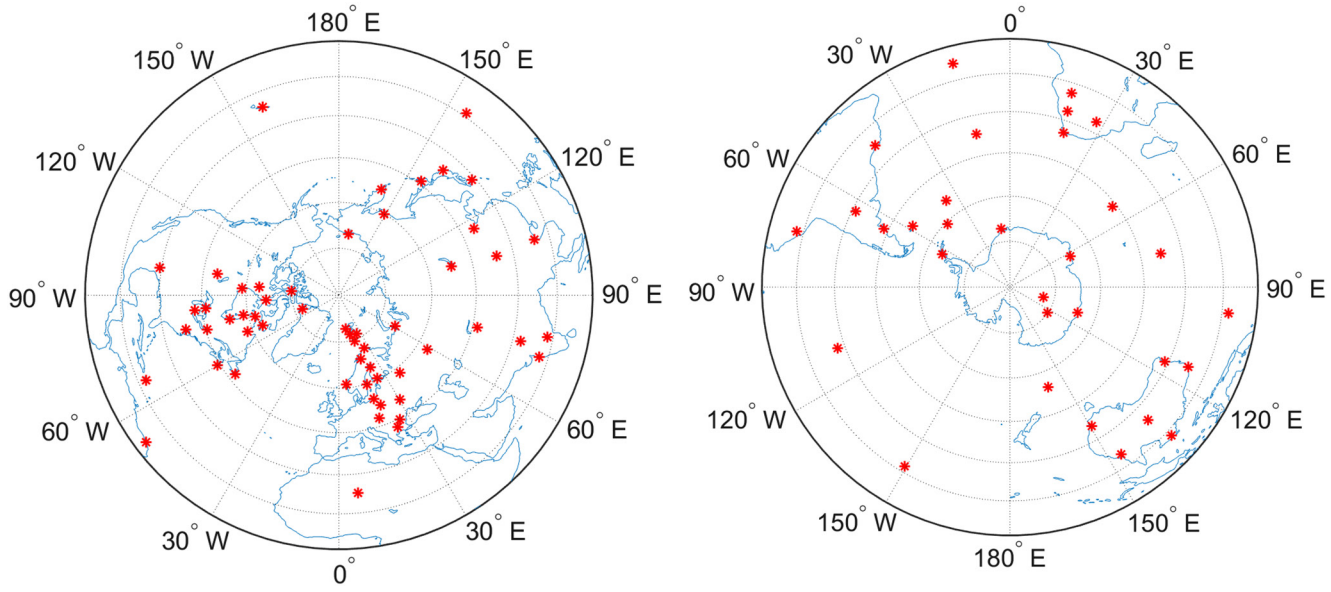

Figure 2. Location of the magnetic stations selected in the Northern (on the left) and Southern (on the right) hemisphere. The distribution is reported in the geographic reference system. The concentric circles represent contours of geographic latitude separated by intervals of 15°.

coordinates (Richmond, 1995), the magnetic local time (MLT) and the original source of data. The selected permanent observatories are part of the worldwide network of observatories known as INTERMAGNET and data can be downloaded at http://www.intermagnet.org/, while the considered magnetometer stations are part of the worldwide network known as SuperMAG (Gjerloev, 2012) and in this case data can be downloaded at http://supermag.jhuapl.edu. All data are validated before using them. Data are checked, spikes are removed and the missing data are identified and linearly interpolated for time intervals less than 5 min. Taking into account that SuperMAG data are provided in the cylindrical coordinate system (H, D, Z), where H is the horizontal component, D is the magnetic declination angle, and Z is the vertical component, while INTERMAGNET data are provided in the local Cartesian coordinate system (X, Y, Z), where X is the North component, Y is the East component, and Z is the vertical component, the two magnetic datasets are standardized expressing all the data in the reference system (X, Y, Z).

3. Method: Empirical Mode Decomposition

The work focus on the analysis of the time fluctuations of the Earth's magnetic field occurring on short timescales (<200 min). To recognize these fluctuations on our original signals we apply the empirical mode decomposition (EMD) method.

This method, introduced by Huang and collaborators (Huang et al., 1996, 1998, 1999) about 20 years ago, has been successfully applied in different fields ranging from the analysis of acoustic signals to biological, oceanic, seismic, and climatological signals (Gloersen & Huang, 1999; Hu et al., 2002; Loh et al., 2001). It has also been applied to geomagnetic time series for example in order to study the multiscale features of intense geomagnetic storms and their possible sources (De Michelis et al., 2012; Alberti et al., 2016, 2017), to extract planetary wave modes from magnetic field components (Frühauff et al., 2015) and to investigate the properties of decadal variations in the length of day (De Michelis et al., 2013; Roberts et al., 2007).

The EMD method starts from the assumption that any non-linear and non-stationary time series can be written as the superposition of simple oscillation modes (the so-called intrinsic mode function, IMF) characterized by different instantaneous frequency values. Since these finite and limited number of IMFs are intrinsic oscillation modes contained in the data, the decomposition of the time series in IMFs allows to directly extract the energy associated with the various timescales intrinsic in the system. The IMFs can be considered as the basis for the expansion of the data and since this basis is constructed from data it can be considered an adaptive basis, and therefore extremely efficient. Each function must satisfy two fundamental conditions to be an IMF. The first condition requires that the number of extremes (maxima and minima) must be equal to the number of crossings of the zero line or at most differ by one in each IMF, while the second condition requires that the mean value between the envelope obtained considering the local maxima and the one obtained considering the local minima must be equal to zero at each instant of time. These two conditions ensure us that there are no superimposed components in the signal, or, in other words, that the signal is a “mono-component” and that the instantaneous frequency of each IMF is not characterized by fluctuations due to an asymmetric wave profile. Consequently, each IMF represents a simple oscillatory mode which is characterized by an amplitude and a frequency that change in time. We used this method to decompose the X and Y components of the Earth's magnetic field recorded at different stations during the selected period. This means that each analyzed time series can be written as follows:

$$\Xi(t) = \sum_i IMF_i(t) + RES(t), \quad \text{where} \quad \Xi(t) = X(t), Y(t). \tag{1}$$

Here, the RES(t) is the residue, that is, a function which has less than two maxima and two minima necessary for the determination of the upper and lower envelopes.

4. Data Analysis and Results

Figure 3 reports an example of the EMD method applied to the Y component of the magnetic field recorded at the Chambon-la-Forêt (CLF) observatory between 13 and 31 March 2015. In detail, Figure 3 reports the 1 min values of the Y magnetic field component at the top, the 15 IMFs obtained by the decomposition in

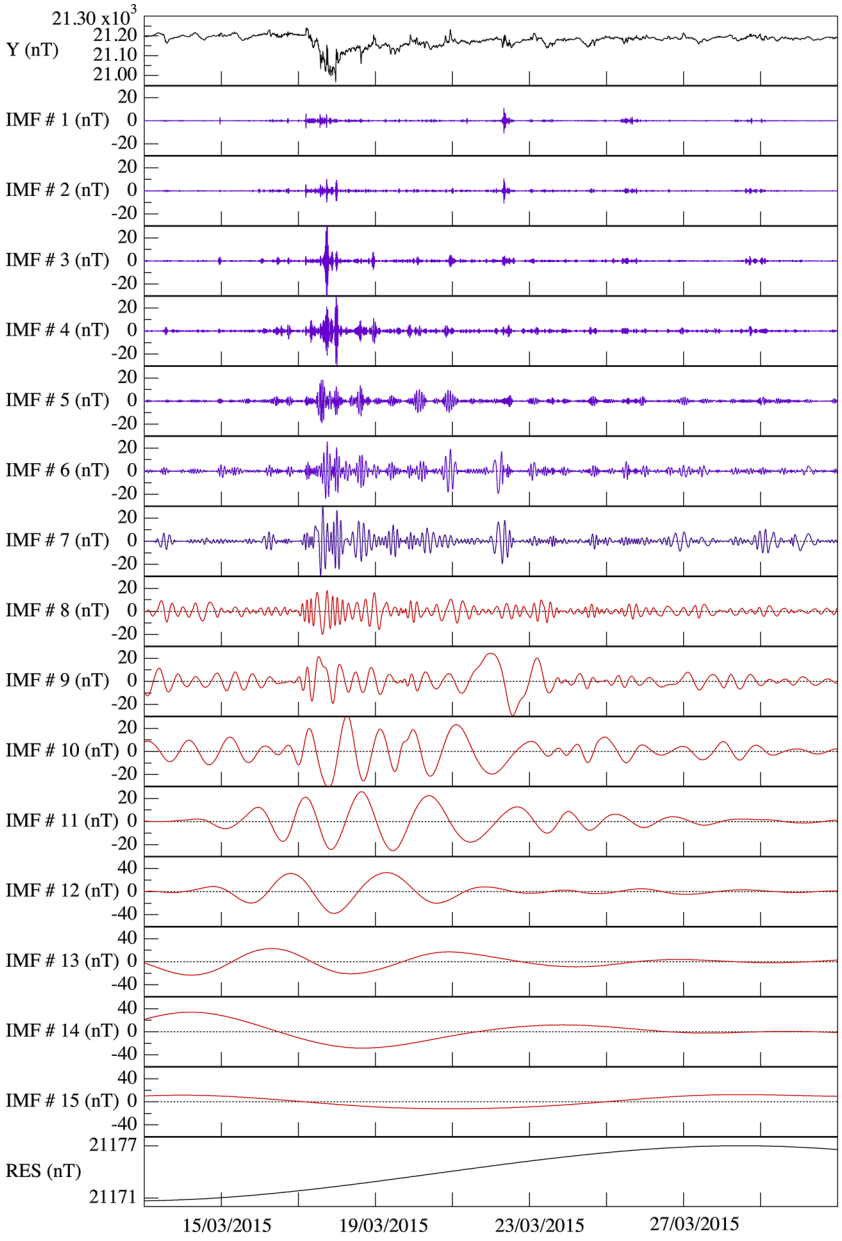

Figure 3. Empirical mode decomposition applied to the Y component of the geomagnetic field recorded at the Chambon-la-Forêt observatory (CLF). In purple the IMFs characterized by average periods $\tau < 200$ min. IMF, intrinsic mode function.

the following plots and the residual term on the bottom. The number of the obtained IMFs is certainly the result of the algorithm used in the analysis but it also depends on the length and complexity of the original time series. This number is usually of the order of $\log_2(N)$, where N is the number of points of the original time series (Flandrin, 2004; Huang & Wu, 2008). In our case, $N = 27{,}360$ (1,440 min × 19 days) and therefore the number of IMFs expected for each analyzed time series is between 14 and 15. This value is in agreement with our results. The number of IMFs obtained on average by decomposing all the time series of our data set is 15.

For each time series, we consider the set of the obtained IMFs and estimate the value of the average frequency associated with each of them. Figure 4 displays the analysis performed on the set of IMFs associated with the magnetic field Y component recorded at the CLF observatory. It reports the Fourier power spectrum

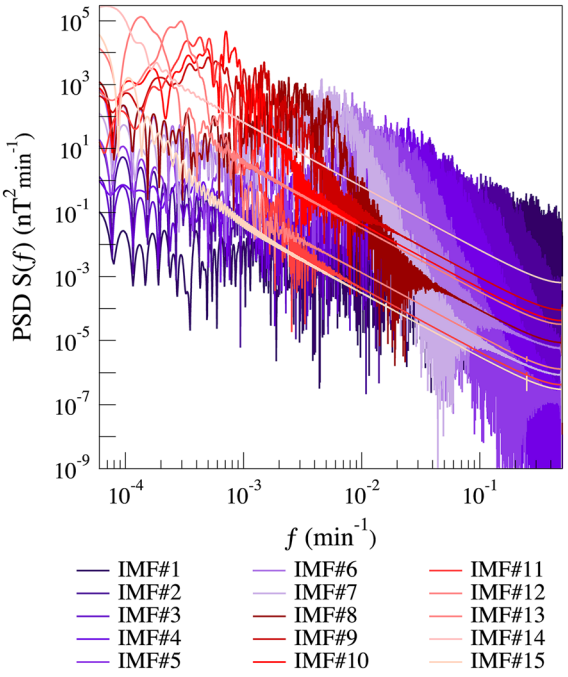

Figure 4. Fourier spectrum of each mode (IMF) identified in the decomposition of the Y component of the magnetic field recorded at the CLF observatory. CLF, Chambon-la-Forêt.

relative to each IMF using different colors. Figure 5 (left panel) shows the value of the average frequency of each mode ($< f_{IMF_i} >$) calculated as the inverse of the average period $< \tau_{IMF_i} >$; the latter is obtained evaluating for each IMF the average distance between the positions of two adjacent maxima ($T^{(k)}_{i,max}$) and two adjacent minima ($T^{(k)}_{i,min}$), respectively, that is, it is defined as

$$\left\langle \tau_{IMF_i} \right\rangle = \frac{1}{2N}\left(\sum_{k=1}^{N-1} (T^{(k+1)}_{i,max} - T^{(k)}_{i,max}) + \sum_{k=1}^{N-1} (T^{(k+1)}_{i,min} - T^{(k)}_{i,min}) \right) \quad (2)$$

The values of the average frequency of each mode ($< f_{IMF_i} >$) reported in Figure 5 (left panel) include the associated standard deviations to represent the spread of data.

Looking at Fourier spectra (Figure 4) and the plot reporting the average frequencies corresponding to the different IMFs (left panel Figure 5) we notice that a wide number of scales is involved in the analyzed magnetic signal. Considering that the range of involved scales covers about three orders of magnitude and the geomagnetic disturbances are the result of electric current systems flowing in different regions of the ionosphere and magnetosphere, we may suppose that the magnetic fluctuations described by the IMFs have different physical properties related to different processes.

The trend of the average frequencies reported in Figure 5 (left panel) shows that EMD method essentially acts as a filter decomposing the signal into a sequence of IMFs characterized, in the Fourier space, by an average frequency that scales according to the law:

$$\left\langle f_{IMF_i} \right\rangle = f_0 \rho^{-i}. \quad (3)$$

where i is the index of the IMF (its order) and f_0 is the characteristic frequency. This result implies that the average frequency of a given mode is ρ times greater than that associated with the immediately following mode. In this case, we obtain $\rho = (1.94 \pm 0.01)$ using the Levenberg-Marquardt least-squares method. Being the obtained value of ρ around 2, the EMD mainly acts as a diadic filter (Flandrin et al., 2004).

To identify the different weight that the IMFs have in the original magnetic signal, we estimate the associated energy, that is, the average power density, of each IMF in terms of its variance (σ^2_{IMF}) and analyze its dependence on the associated average frequency. Indeed, given an oscillating signal, such as a sinusoidal

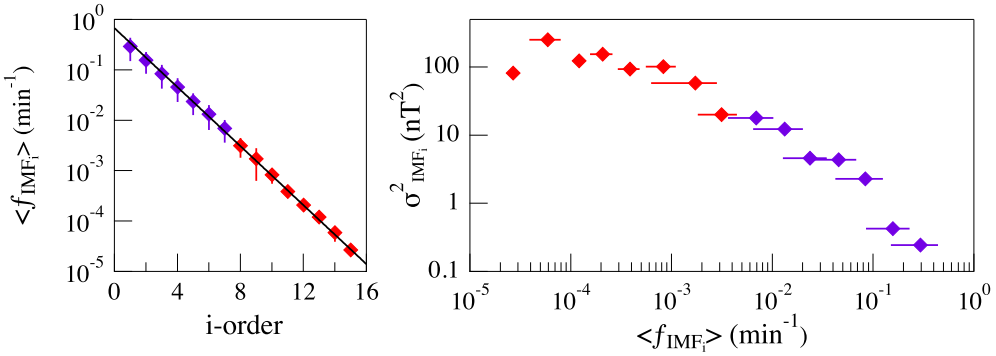

Figure 5. Left: Average frequency values of each IMF obtained from the decomposition of the Y component of the magnetic field recorded at the CLF observatory and reported in Figure 3. Right: Variance of each IMF as a function of its average frequency. CLF, Chambon-la-Forêt; IMF, intrinsic mode function.

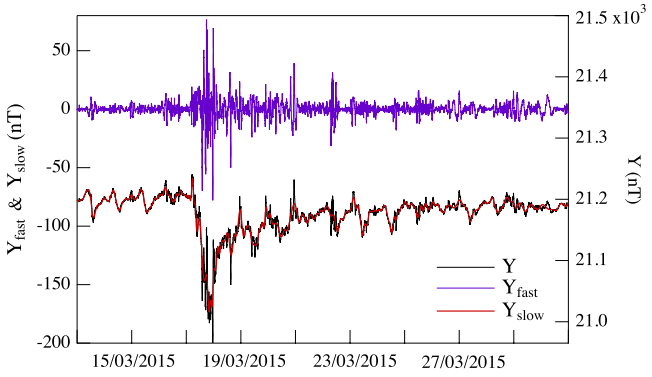

Figure 6. An example of the different magnetic signals (Y_{fast} [purple line] and Y_{slow} [red line]) identified in the magnetic field Y component (back line) recorded at the CLF observatory. CLF, Chambon-la-Forêt.

one, its instantaneous average energy, or the average energy per time, is provided by the mean squared value of its amplitude, that is, its second moment. The second moment of a signal corresponds with its variance in the case of a signal with zero mean as it is for the IMFs.

The results are shown in the plot on the right panel of Figure 5. According to Alberti et al. (2017), we have organized the IMFs in two different groups characterized by $\tau \lessgtr 200$ min, respectively. The values reported in red refer to IMFs with an average estimated period $\tau > 200$ min while those in purple refer to IMFs characterized by $\tau < 200$ min. All the IMFs characterized by $\tau > 200$ min constitute 94% of the total signal (in terms of energy) while those characterized by $\tau < 200$ min constitute only 6% of the original one. The same analysis repeated on the X component recorded at the same geomagnetic observatory (data not shown) reveals a slight different result, the IMFs with $\tau > 200$ min constitute 85% of the total magnetic signal while the others constitute its 15%. These values are referred to the fluctuating part of the original magnetic signal obtained by removing the residual term from it. Indeed, the residual term is not an IMF and, for this reason, it is not considered in our analysis. However, we notice that the residual term essentially describes the contribution to the original signal due to the so-called main field, that is, the magnetic field produced by all sources within the Earth and its very long-term trends, which are not relevant to our purposes. When we remove the residual term from our original magnetic signal we can study the magnetic effects on the ground due to sources which are external to the Earth, that is, due to those current systems flowing in the ionosphere and magnetosphere. This means that the previous percentages refer to the fluctuating part of the external magnetic field.

Considering the values of the average frequency associated with each IMF we can decompose our time series in two different signals. The first magnetic signal is obtained from the superposition of all the IMFs characterized by an average frequency greater than 5×10^{-3} (min^{-1}), that means $\tau < 200$ min. We indicate this fraction of the fluctuating part of the original magnetic signal as "fast" component. In the case of the Y component recorded at the CLF observatory, there are seven IMFs characterized by average frequencies above the fixed threshold. They are identified by purple color in Figure 3 and their superposition represents the "fast" component of the original magnetic signal. The others eight IMFs are characterized by average frequencies below the fixed threshold and they are identified by red color in Figure 3. Their superposition is the "slow" component of the fluctuating part of the original magnetic signal.

Figure 6 shows an example of these two different magnetic signals identified in the magnetic field Y component recorded at the CLF observatory. In detail, it reports a comparison among the fast (Y_{fast}), the slow (Y_{slow}) and the original Y component. The Y_{fast} and Y_{slow} components are reported on the left axis of the plot using the same scale while the original Y component is reported on the right axis of the same plot. The periodic variation observed in both the original (Y) and the slow (Y_{slow}) magnetic components is the well-known solar quiet daily variation, which mainly arises from the ionospheric current system flowing in the so-called dynamo region.

The analysis is repeated for all the time series of our data set, that is, we decompose the X and Y components recorded at the selected magnetic stations and identify the fast and slow contributions for each of them after removing the residual term. Considering that any magnetic station co-rotates with the Earth, each of them spans 360° in 1 day moving along an ideal circumference around the pole. Using magnetic stations located at different latitudes and taking into account data recorded in a whole day we have a good latitudinal coverage which permits us to obtain a good daily representation of the external magnetic field and of its fast and slow fluctuating parts. For each day, indeed, we reduce all the data recorded at each selected magnetic station with a time resolution of 1 min on a regular grid (1.5° × 1.5°) and apply the weighted Gaussian interpolation scheme as described in De Michelis and Consolini (2015). In detail, using all the available daily data consisting of the magnetic field components as function of latitude and magnetic local time, we compute the local value on the map grid averaging data with a weight that is a function of the distance between the grid point and the available data coordinates, that is,

$$\overline{Z}(x,y) = \frac{\sum_{i=1}^{n} \hat{k}(x - x_i, y - y_i) Z(x_i, y_i)}{\sum_{i=1}^{n} \hat{k}(x - x_i, y - y_i)}, \quad (4)$$

where (x, y) are the coordinates of the grid point, (x_i, y_i) are the coordinates of the available data, $Z(x_i, y_i)$ is the quantity to be averaged, $\overline{Z}(x,y)$ is the resulting average value at the point (x, y), and $\hat{k}(x - x_i, y - y_i)$ is the used weighting function, that is,

$$\hat{k}(x - x_i, y - y_i) = \exp\left[-\frac{(x - x_i)^2 + (y - y_i)^2}{2d_{xy}^2}\right] \quad (5)$$

where d_{xy} is the weighting function amplitude, which is set to be of the order of 2.5°. In this way, we reduce possible artifacts due to a nonuniform spatial distribution of data. Clearly, this method operates a smoothing of the available information, which depends on the width of the weighting function.

Figure 7 displays an example of the obtained results. We focus on 5 days around the St. Patrick's Day storm showing polar view daily maps of the fluctuating part of the original magnetic signal in the case of the X and Y components recorded in the Northern hemisphere. The fluctuating part of the original magnetic signal is obtained by removing the residual term from the original magnetic signal and describes, as we mentioned above, the magnetic field of external origin. Data are shown using a polar representation in magnetic coordinates, and more exactly in QD-latitude and magnetic local time (MLT) reference system. The choice of this magnetic reference system is made because the QD coordinates are particularly suitable for describing horizontally stratified phenomena occurring in the ionosphere (Emmert et al., 2010), while the introduction of MLT allows an organization of data with respect to the Sun position. The MLT is calculated according to the definition by Baker and Wing (1989). The polar view daily maps reported in Figure 7 describe the magnetic effect on the ground due to ionospheric and magnetospheric current systems which change their intensity and partially their location with the geomagnetic activity. The maps show the magnetic effect on the ground mainly due to two different electric current systems: the auroral electrojet and the ring current. The first electric current system characterizes the high-latitude ionospheric regions and reflects the auroral response to the changes of the interplanetary magnetic field and solar wind parameters. This current system shifts equatorward during periods of high geomagnetic activity as can be observed also in our maps. During the main phase of the analyzed storm the westward electrojet, which produces a decrease in the X component of the magnetic field on the ground, covers the latitudes from 50° and 70° on the nightside (22:00 < MLT < 05:00) while the eastward electrojet, which produces an increase in the X component of the magnetic field on the ground, can be recognized in the dusk sector (13:00 < MLT < 19:00) at latitudes lower than those of the westward electrojet. The intensity of these two currents changes during the analyzed period reaching the maximum value during the main phase of the magnetic storm occurred on March 17, 2015. At lower latitudes, during the main phase of the storm, it is also possible to notice the contribution to the magnetic field of external origin due to the ring current. It flows around the Earth in the westward direction on the magnetospheric equatorial plane at a distance between 5 and 8 Earth radii, and can be considered as the dominant signature of geomagnetic storms. It is responsible of a depression in the magnetic field horizontal component lasting from one to several days. Daily maps relative to 17 and 18 March report a negative magnetic field between 20° and 40° and 18:00 < MLT < 06:00 in the X component which reflects the effect on the ground of this equatorial current system. We note that the auroral electrojet remains particularly intense even in the days following the main phase of the storm. During the recovery phase of the storm, the mid-/high-latitude regions (>50°) are characterized by the occurrence of a series of magnetospheric substorms, as can be observed looking at the temporal trend of the AE index, that feed the auroral electrojet intensity producing the magnetic field variations recorded on the ground.

Starting from the fluctuating part of the original magnetic signal in the case of the X and Y components we investigate its fast and slow components. Figure 8 displays an example of the obtained results in the Northern hemisphere. Here, always focusing on the 5 days around the St. Patrick's Day storm, we report polar view daily maps of the contribution (in terms of percentage) of the fast fluctuations to the external signal in the case of the X and Y components, respectively. To compare the obtained results we evaluate for each magnetic station and each magnetic field component the ratio between the average energy (in terms of variance)

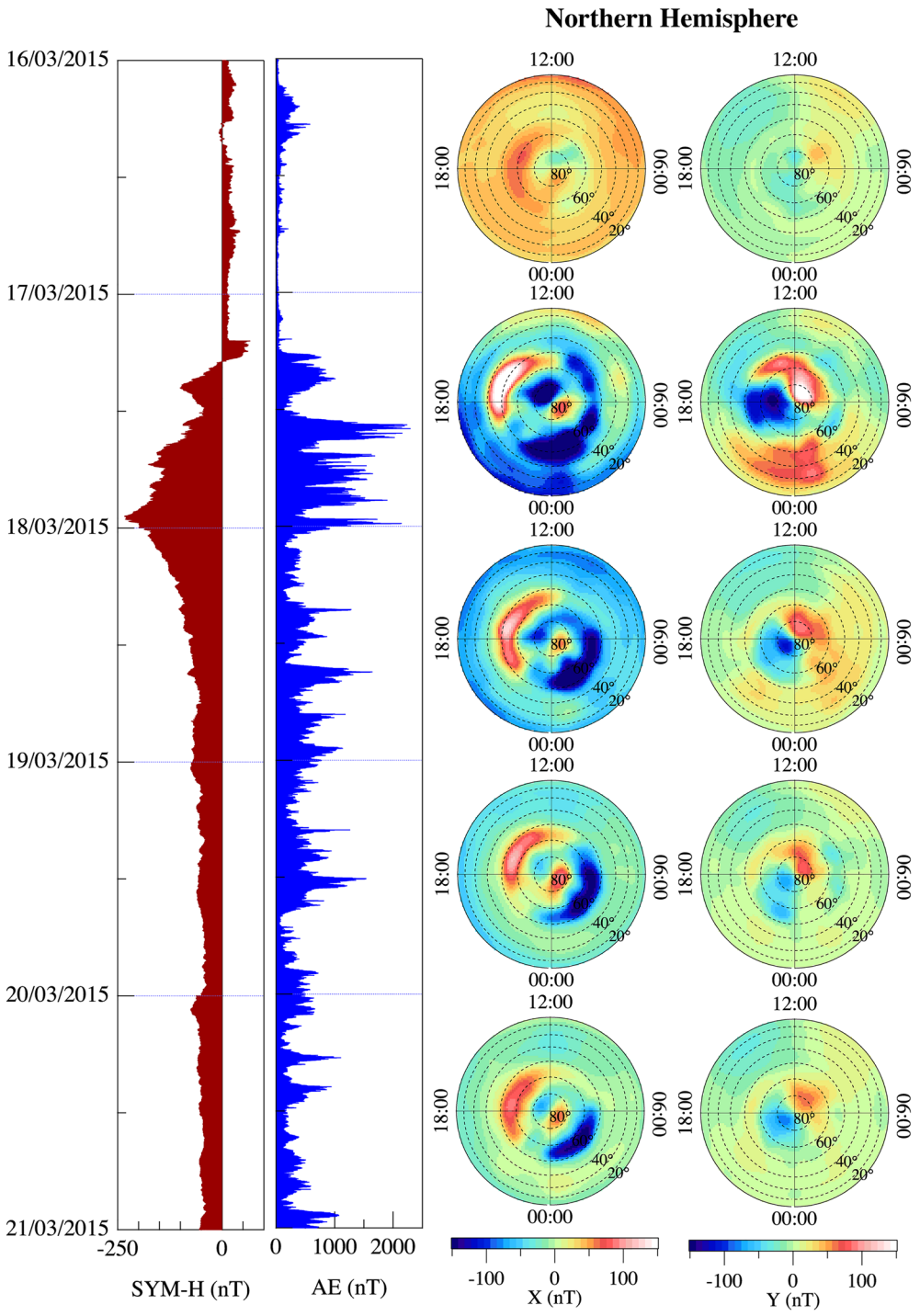

Figure 7. On the left SYM-H and AE indices; in the other two columns, daily polar view maps of the magnetic field of external origin along the X and Y components in the Northern hemisphere. Data are reported in magnetic latitude (from 20° to 90°) and MLT coordinate system, the concentric circles represent contours of magnetic latitude, separated by intervals of 10°. Maps refer to a period of 5 days from 16 to 20 March 2015. MLT, magnetic local time.

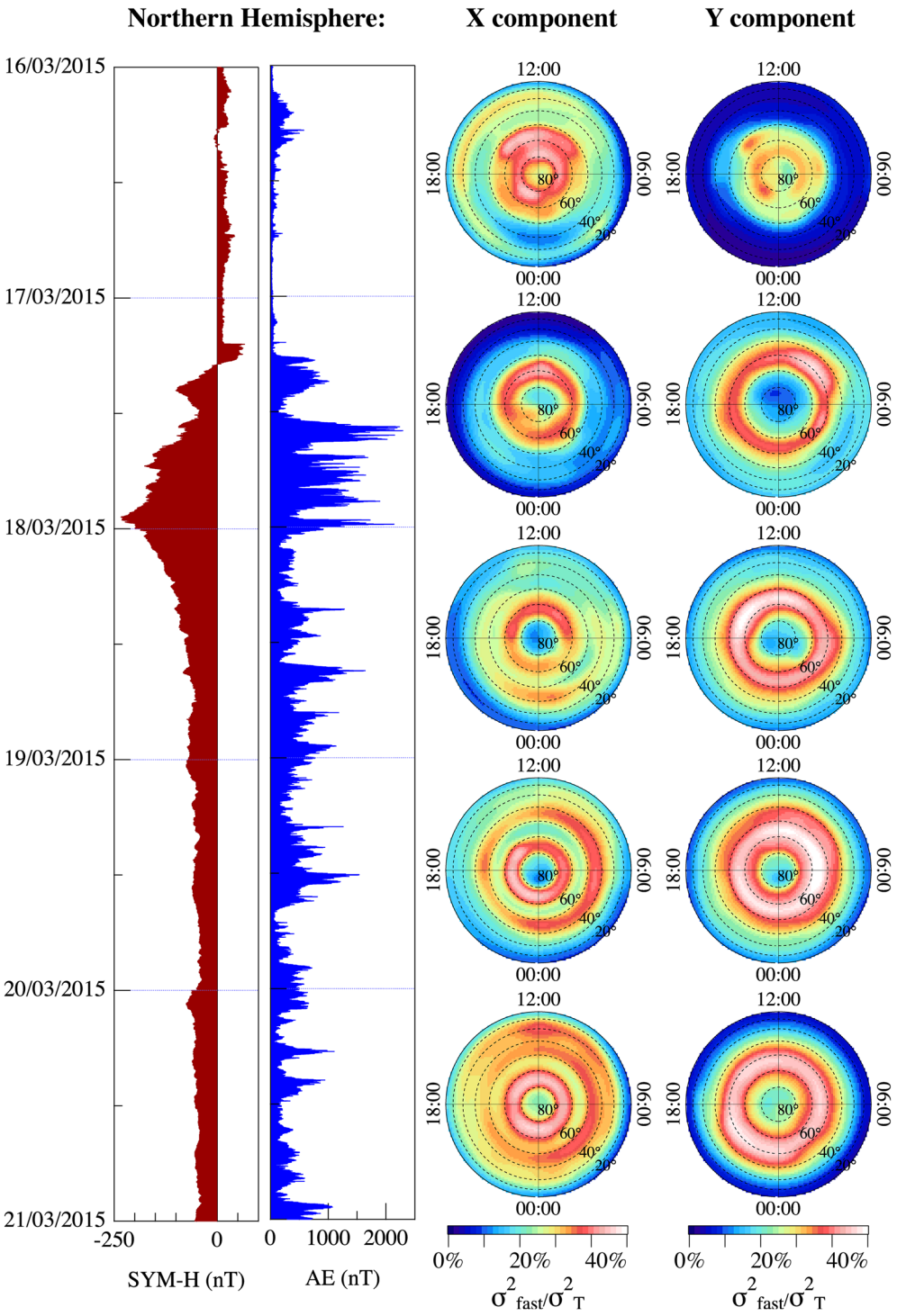

Figure 8. On the left SYM-H and AE indices; in the other two columns, daily polar view maps of the fast fluctuation contributions ($\tau < 200$ min) to the external magnetic field for the X and Y components in the Northern hemisphere. Data are reported in magnetic latitude (from 20° to 90°) and MLT coordinate system, the concentric circles represent contours of magnetic latitude, separated by intervals of 10°. Maps refer to a period of 5 days from 16 to 20 March 2015.

of the fast fluctuating part of the signal (σ^2_{fast}) and the average energy associated with the total fluctuating magnetic signal (σ^2_T). These values are computed on a moving window of 1 day. The ratio between these two variances (σ^2_{fast} / σ^2_T) permits us to describe the contribution of the fast fluctuating part of the signal to the total one in terms of its percentage. We evaluate the same quantity also in the case of the slow fluctuating part (σ^2_{slow} / σ^2_T). To analyze the spatial and temporal evolution of the contribution given by the fast and slow fluctuations to the external magnetic signal we study the σ^2_{fast} / σ^2_T and σ^2_{slow} / σ^2_T ratios as a function of magnetic latitude and magnetic local time over daily windows. A preliminary analysis of the obtained daily maps shows how the σ^2_{fast} / σ^2_T values depend on the geomagnetic activity level which is described by the two geomagnetic indices, SYM-H and AE, reported on the left of Figure 8. These variations characterize both magnetic field components. We note that the percentage refers to the single analyzed component (X and Y), while the relative weight of one component in relation to the other is not taken into account.

The daily maps relative to the Y magnetic field component reveal that, during magnetically quiet days (such as for example on March 16, 2015), the fast magnetic fluctuations contribute to the external magnetic signal essentially at high latitudes (>60°) where about 25% of it is due to fast fluctuations. Otherwise, at mid and low latitudes (<60°) the same fast fluctuations seem almost not to contribute to the external signal. A similar result is obtained in the case of the X component with the only difference that at mid and low latitudes the contribution to the external signal from fast fluctuations is on average higher (values between 10% and 15%) than obtained in the case of the Y component. Therefore, the two magnetic field components do not seem to respond to fast external fluctuations in the same way. In any case, when the magnetic activity level increases, the region characterized by a magnetic signal where the fast fluctuations play an important role tends to extend toward lower latitudes. At high latitudes the maximum σ^2_{fast} / σ^2_T values seem to identify the position of the auroral oval. In this area, in the case of the Y component, the contribution in terms of energy of fast fluctuations to the external signal reaches 50%. This is true during the main phase of the storm and its recovery phase when the high-latitude regions are characterized by the occurrence of many substorms. However, the latitudinal ranges of the maxima of the fast contribution for the X and Y components of the field do not exactly match. The sigma ratios for the X component maximize at 70°–80°, while the same ratios for the Y component maximize below 70°. A possible explanation of such features could be the effect of non-vertical field-aligned currents (FACs), which according to Tamao (1986) generate a non-vanishing East-West contribution to the ground magnetic field, that is, to the Y component.

The regions affected by an increase in the contribution of the fast magnetic fluctuations to the total signal are characterized by the presence of the auroral electrojet current system. As we mentioned earlier, it is one of the most important current system at auroral latitudes and consists of two different currents that rotate eastward and westward, respectively. These two current systems intensify during magnetically perturbed periods and are known to move drastically toward the equator during geomagnetically disturbed periods. The area where the fast fluctuations mostly contribute to the total signal seems to follow the dynamics of this current system suggesting that the maximum contribution of fast fluctuations to the magnetic signal seems to happen in correspondence with the auroral oval. To investigate this relationship, we consider the horizontal part of the ground magnetic disturbance of external origin. This can be mainly considered as the signature of the ionospheric and magnetospheric current systems on the ground. That means to calculate the horizontal intensity (H) of the magnetic field, which is given by $H = \sqrt{(X^2 + Y^2)}$, and to evaluate the contributions due to the fast and slow magnetic fluctuations, respectively.

Figure 9 reports the daily polar view maps (16–20 March 2015) of σ^2_{fast} / σ^2_T relating to the intensity of the H magnetic field component in the Northern hemisphere. In the same figure we report also the daily polar view maps of σ^2_{slow} / σ^2_T relating to the same component in order to make a comparison between the spatial and temporal distributions of the fast and slow contributions to the external magnetic signal. The maximum contribution of fast fluctuations to the intensity of the H magnetic field component is concentrated at high latitudes and its distribution on the QD Lat–MLT plane depends on magnetic activity. Conversely, the maximum contribution of slow fluctuations is concentrated at mid and low latitudes and also in this case it is a function of geomagnetic activity level. In any case, there are some very high values of the contribution of the slow fluctuations in the central polar cap, mostly during the peak of the storm. According to Alberti et al. (2017), this suggests the activation of processes that should be directly driven by the solar wind and

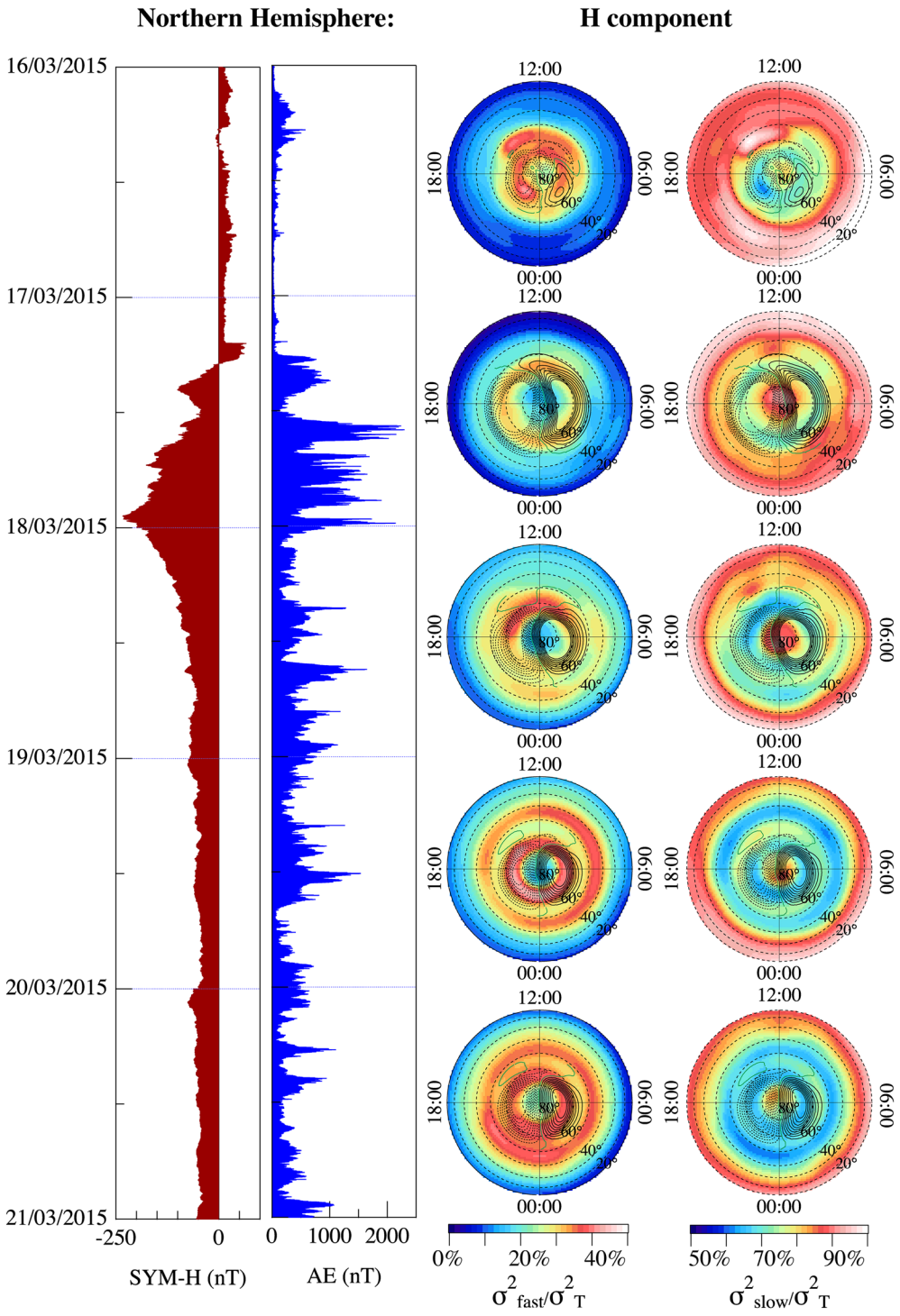

Figure 9. On the left the evolution of the SYM-H and AE indices; in the other two columns, daily polar view maps of the contribution of the fast ($\tau < 200$ min) and slow ($\tau > 200$ min) fluctuations to the intensity of the magnetic field H component in the Northern hemisphere. Superposed to magnetic field maps the SuperDARN polar potential maps obtained using the statistical convection model CS10. Data are reported in magnetic latitude (from 20° to 90°) and MLT coordinate system, the concentric circles represent contours of magnetic latitude, separated by intervals of 10°. Maps refer to the period 16–20 March 2015. MLT, magnetic local time.

interplanetary magnetic field changes. The features observed in the region near the pole (>80°), which corresponds to the antisunward part of the two-cell convection pattern, are mainly due to data recored at two magnetic stations, RES and THL. Here, the THL station, is used to derive the geomagnetic Polar Cap (PC) index, which is known to show a good correlation with the solar wind parameters. Thus, we should not be too surprised by the feature we have found. This region is less affected by the internal dynamics of the magnetosphere than the surrounding areas, and seems to be more directly driven by the solar wind changes. Moreover, it is important to remember that this region, which corresponds roughly to the poleward boundary of the auroral oval, is characterized by the presence of open magnetic field lines and consequently it is more subject to the direct influence of the solar wind and interplanetary magnetic field changes.

To estimate the correspondence between the location of the regions characterized by the maximum contribution of the fast fluctuations to the magnetic signal of external origin and the auroral oval region, we reconstruct the plasma convection cells using the CS10 model (Cousins & Shepherd, 2010). This is a dynamic statistical convection model obtained from SuperDARN (Super Dual Auroral Radar Network), a network of 35 high-frequency radars located on the ground, that calculates the distribution of high-latitude plasma convection patterns organized by solar wind, interplanetary magnetic field, and dipole tilt angle conditions. Using this model, for each selected day, we evaluate the average daily values of the solar wind velocity and interplanetary magnetic field conditions in order to derive the corresponding convection patterns. The results obtained are superimposed on our daily polar view distributions as shown in Figure 9. The cells reach their maximum spatial extension during the main phase of the storm but they remain expanded for 12 h after the main phase. The comparison between the two-cell plasma convection patterns and the spatial-temporal distribution of σ^2_{fast} / σ^2_T relating to the intensity of the H magnetic field component seems to confirm the initial idea according to which the maximum contribution of fast fluctuations to the magnetic signal of external origin on ground is essentially inside the auroral oval on the equatorward side of convection cells, while the polar cap is mainly affected by slow fluctuations, which are mainly directly driven by solar wind and IMF changes.

We obtain similar results analyzing the magnetic data recorded by stations located in the Southern hemisphere. Figure 10 displays daily polar view maps of the contribution of the fast ($\tau < 200$ min) and slow ($\tau > 200$ min) fluctuations to the intensity of the magnetic field H component in the same time interval (16–20 March 2015) reported in Figure 9. A reduced number of magnetic stations were used in the Southern hemisphere due to the geographically restricted land cover of stations in this hemisphere. The obtained results show a slight difference between the two hemispheres. The difference is mainly concentrated at high latitude in correspondence with the auroral oval region. The contribution of fast field fluctuations to the external magnetic signal is higher in the Southern hemisphere than in the Northern one. The asymmetry between the two hemispheres can be partly attributed to the asymmetry of the Earth's magnetic field which, as it is known, involves the asymmetry in ionospheric convection, ionospheric winds, electron density, auroral emissions, and ionospheric conductivity (Laundal et al., 2016). A different ionospheric conductivity necessarily implies a difference in ionospheric currents and magnetic perturbations associated with them. Nevertheless, we cannot exclude that this difference may be due to a lower coverage of magnetic stations and consequently to a worse statistics. Furthermore, by comparing North and South polar maps on the pre-storm day (16 March) we note a strong apparent cusp region which is located at post-noon MLTs in the Northern hemisphere and at pre-noon MLTs in the Southern one.

The Lastly, to highlight the dependence on geomagnetic activity level of the fast fluctuations to the external magnetic field Figure 11 displays the daily polar view maps of σ^2_{fast} / σ^2_T relating to the intensity of the H magnetic field component in correspondence with three different days. The selected days are characterized by different levels of geomagnetic disturbance: a quiet day (14 March), a strongly disturbed day (17 March), and a moderate disturbed day (25 March). The comparison among the maps shows how the contribution of fast fluctuations to the external magnetic signal strongly depends on the geomagnetic activity level. According to geomagnetic disturbance, the contribution in terms of percentage to the total magnetic signal changes as the location of the regions in which these fluctuations play a significant role changes.

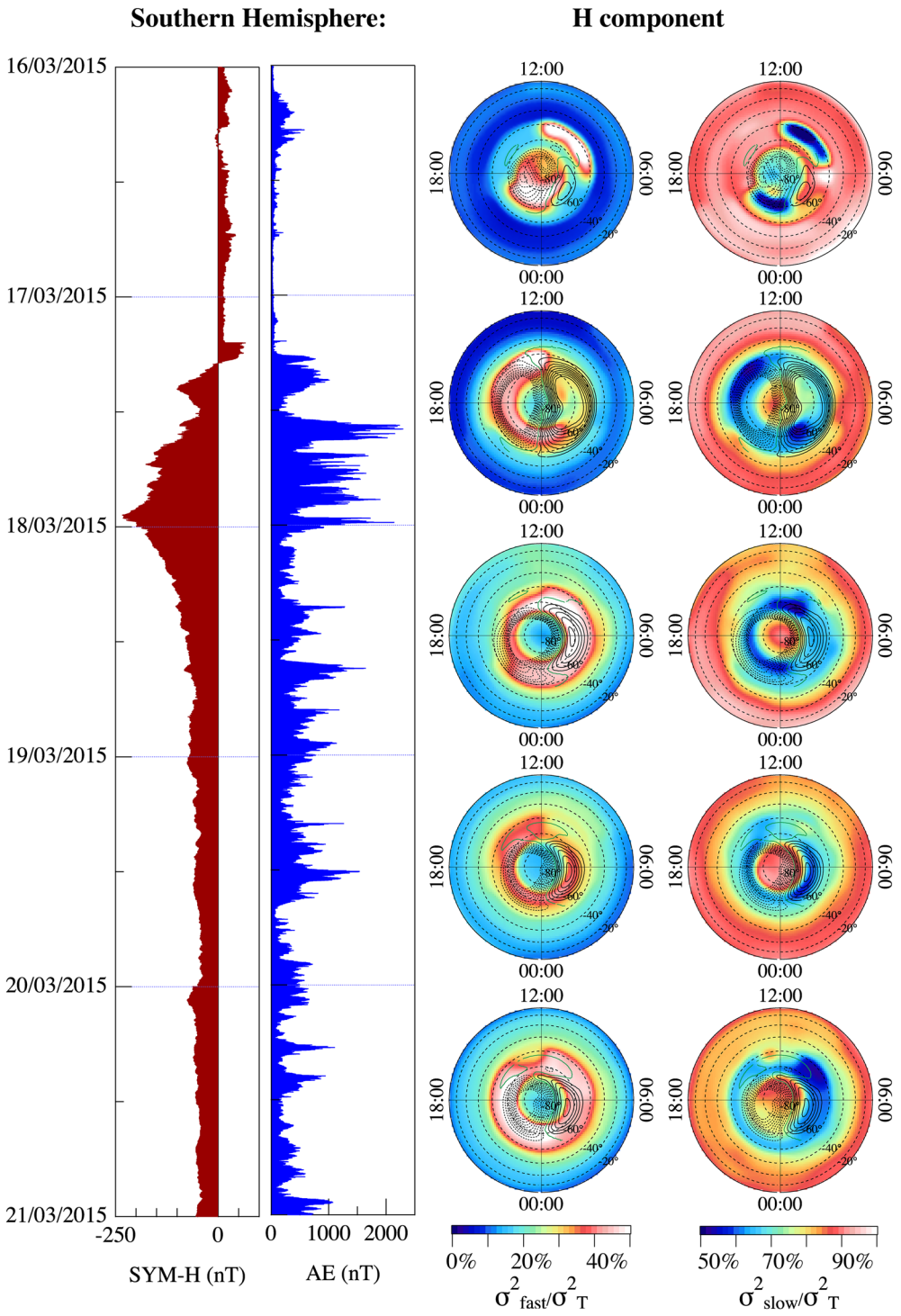

Figure 10. On the left the evolution of the SYM-H and AE indices; in the other two columns, daily polar view maps of the contribution of the fast ($\tau < 200$ min) and slow ($\tau > 200$ min) fluctuations to the intensity of the magnetic field H component in the Southern hemisphere. Superposed to magnetic field maps the SuperDARN polar potential maps obtained using the statistical convection model CS10. Data are reported in magnetic latitude (from 20° to 90°) and MLT coordinate system, the concentric circles represent contours of magnetic latitude, separated by intervals of 10°. Maps refer to the period 16–20 March 2015. MLT, magnetic local time.

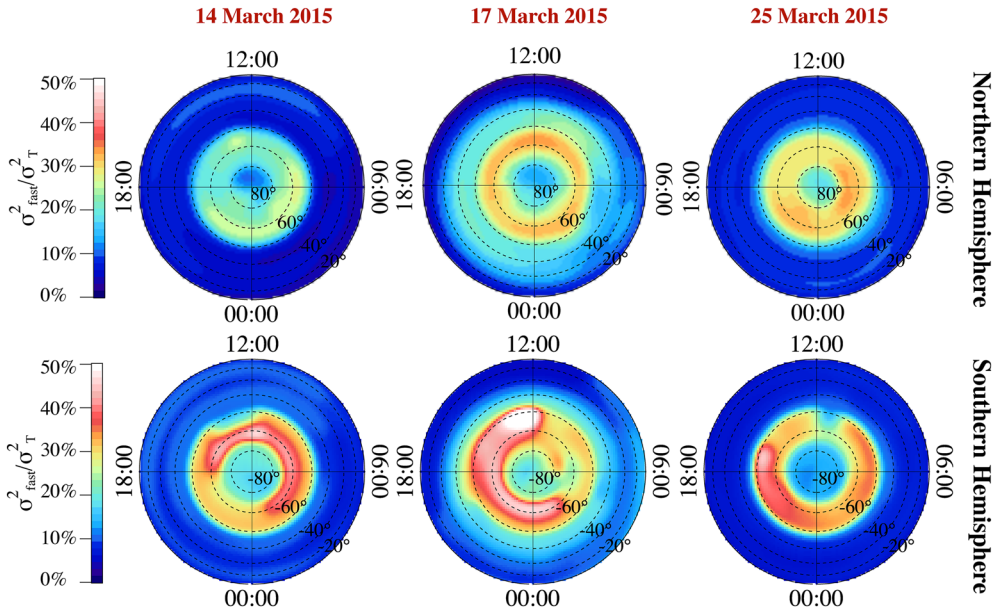

Figure 11. Daily polar view maps of the contribution of the fast ($\tau < 200$ min) fluctuations to the intensity of the magnetic field H component in the Northern and Southern hemispheres during 3 days characterized by different geomagnetic activity levels. Data are reported in magnetic latitude (from 20° to 90°) and MLT coordinate system, the concentric circles represent contours of magnetic latitude, separated by intervals of 10°. MLT, magnetic local time.

5. Summary and Conclusions

The aim of this work was to study the nature of the fluctuations at different timescales of the Earth's magnetic field recorded on the ground in order to understand their dependence on magnetic latitude, magnetic local time and geomagnetic activity level. For a period of 19 days (13–31 March 2015) we considered magnetic data recorded along the two horizontal (X and Y) components of the geomagnetic field at 78 magnetic stations belonging to worldwide networks of stations (INTERMAGNET and SuperMAG) and selected so as to guarantee the widest possible latitude and longitude coverage. We applied the EMD method to study detailed structures of the time series of magnetic field fluctuations as they consist of non-linear and non-stationary processes. The method permitted us to separate the original time series in simple oscillation modes characterized by different instantaneous frequencies and to associate the original magnetic signal with a superposition of three terms: The first term describes the magnetic fluctuations characterized by periods $\tau < 200$ min, the second term describes the magnetic fluctuations with periods $\tau > 200$ min and the third term is the residue. This last term describes the contribution to the original signal due to the main field and to its long term variations such as the seasonal and secular variation, while the other two terms altogether describe the magnetic field of external origin. We focused on the magnetic signal of external origin characterized by fast fluctuations ($\tau < 200$ min) and analyzed its dependence on magnetic latitude, magnetic local time, and magnetic activity level. The analysis showed that the greatest magnetic contribution to the external magnetic signal from fast fluctuations is concentrated mainly at high latitudes in the auroral oval region, where on average more than 30% of the magnetic signal is due to fast field fluctuations.

In detail, the maximum contribution of fast fluctuations to the external magnetic signal seem to occur along the auroral oval on the equatorward side of the plasma circulation cells, that is, in those high-latitude regions which essentially map into the near-Earth magnetotail equatorial regions on the nightside. We suggest that one of the possible sources of these fast fluctuations, especially in the nightside, is the turbulent and bursty dynamics of the central magnetotail, where fast and sporadic energy releases have been observed due to occurrence of localized reconnection/relaxation processes, which mainly take place during magnetospheric substorms (Angelopoulos et al., 1999; Lui et al., 1998). The bursty dynamics is, indeed, related to the so-called loading-unloading process that is one of the features of magnetospheric substorms, which is mediated by the local conditions of the magnetotail central plasma sheet (CPS). One of the features of the

unloading component of auroral electrojet current system is that this bursty dynamics is essentially characterized by timescales below 100 min (Consolini & De Michelis, 2005; Kamide & Kokubun, 1996; McPherron et al., 1973). Furthermore, this dynamics is mainly due to the internal rearrangement of the CPS state, which is only triggered by the changes of the interplanetary conditions. This scenario is supported by previous studies that clearly showed how the CPS and the magnetotail are characterized by a multiscale, turbulent and near-criticality dynamics (Borovsky et al., 1997; Consolini & Chang, 2001; Consolini et al., 1996; Klimas et al., 1996; Uritsky et al., 2002; Zimbardo et al., 2010). For instance, Lui et al. (1998) showed that some sporadic and localized plasma energizations and magnetic flux transport occur in the magnetotail regions in coincidence with auroral breakups. Furthermore, according to Alberti et al. (2017), during the St. Patrick's Day storm, the fluctuations of auroral electrojet current systems at timescales shorter than 200 min do not show any significant correlation with solar wind fluctuations at the same timescales. Consequently, these fluctuations have to be mainly related to the internal magnetospheric processes. At timescales below 200 min, these observations are consistent with the nonlinear and near-criticality response of the Earth's magnetosphere to solar wind and interplanetary changes as found by Tsurutani et al. (1990) and Uritsky et al. (2001).

On the other hand, the auroral oval region is subjected to variations in the magnetic latitude–MLT plane which depend on the geomagnetic activity level. It contracts around the magnetic pole during quiet periods, while it expands toward lower latitudinal values during disturbed periods. These dynamical features characterize also the region where the fast magnetic field fluctuations most contribute to the total magnetic signal permitting us to suppose that they can be essentially related to the rapid enhancement of the overall auroral electrojet (eastward and westward) current system both in the nightside and in the dayside regions, whose intensities, as well as location, strongly depend on magnetic activity level. As well documented in the literature, the enhancement of this electric current system is closely associated with the magnetospheric plasma dynamics (transport and energization) during the occurrence of magnetic storms and substorms, and is generated by different sources such as the large-scale convection in the magnetosphere, the increase in field aligned currents due to the disruption and diversion of the cross-tail magnetospheric current and the development of the partial ring current (Feldstein et al., 2006). All these processes are clearly the result of the internal magnetospheric dynamics, which is triggered by the solar wind and the interplanetary magnetic field. The effect of auroral electrojet current system on the magnetic signal of external origin recorded on the ground is remarkable. During the main phase of the storm and in the days immediately following it the contribution of fast magnetic field fluctuations to the recorded magnetic signal of external origin can reach 50% in terms of energy.

This is a crucial aspect in the framework of mitigation of Space Weather effects, such as the occurrence of geomagnetically induced currents (GICs). These currents flowing on electrically conducting systems on the ground can compromise the integrity and performance of some important modern infrastructures, such as telecommunication cables, power grids, railway systems, and pipelines (Ngwira & Pulkkinen, 2019). They are generated by fast variations of the magnetic field (dB/dt) on the ground, so that fast magnetic fluctuations may have a great relevance on it. Global magnetohydrodynamics, empirical and numerical models (see for example Pulkkinen et al., 2011; Weimer, 2013, 2019, Welling, 2019) have been developed in the past to model and forecast geomagnetic perturbations at ground level responsible of GICs. However, while these models are capable of predicting the low-frequency variations in the magnetic field, they are unable to reproduce the high-frequency fluctuations and fast substorm perturbations that is, fluctuations at time scale shorter than 5 min. Although this aspect can be in some cases negligible, it is fundamental in order to successfully model and forecast the amplitude of geomagnetically induced currents which strongly depends on magnetic time derivative changes. The fast component of magnetic fluctuations must be in someway incorporated into these models to result in a more significant space weather prediction with a special emphasis on GIC predictions in the auroral zones. Indeed, the fast component of magnetic fluctuations, which includes chaotic, high-frequency fluctuations and fast substorm variations can reach 50% in terms of energy to the total magnetic signal.

Appendix A: List of Selected Magnetic Stations

Table A1 presents information on selected magentic stations.

Table A1
Selected Magnetic Stations: IAGA Identification Code, Geographical and Quasi-Dipole Magnetic Coordinates, Magnetic Local Time (MLT), and the Source of Data (I=INTERMAGNET, S=SuperMAG)

IAGA code	Lat (°N)	Long (°E)	QDLat (°N)	QDLong (°E)	MLT (hr)	Source
AAA	43.20	76.90	39.45	150.50	4.82	I
ABG	18.62	72.87	12.87	146.50	4.56	I
ABK	68.36	18.82	65.55	100.43	1.49	I
AIA	−65.25	295.75	−51.31	19.45	9.89	I
AMD	69.50	61.40	66.02	137.82	3.98	I
AMS	−37.80	77.57	−48.93	141.22	4.21	I
ARS	56.43	58.57	53.15	132.50	3.62	I
ASP	−23.77	133.88	−33.62	151.58	8.69	I
BEL	51.84	20.79	47.73	96.01	1.19	I
BLC	64.32	263.99	72.70	−28.02	16.92	I
BJN	74.50	19.20	71.80	105.85	1.85	S
BMT	40.30	116.20	35.53	−169.16	7.51	I
BOX	58.07	38.23	54.64	113.22	2.34	I
BRD	49.87	260.03	58.73	−31.47	16.69	I
CKI	−12.19	96.83	−21.54	169.59	6.10	I
CNB	−35.32	149.36	−45.17	−131.85	10.00	I
CSY	−66.28	110.53	−80.62	160.71	5.51	I
CTA	−20.10	146.30	−29.06	−138.25	9.57	I
C01	42.42	276.10	52.22	−8.37	18.23	S
FCC	58.76	265.91	67.66	−23.97	17.19	I
FRD	38.20	282.63	47.58	0.56	18.83	I
GNG	−31.36	115.72	−42.61	−171.76	7.34	I
GUA	13.59	144.87	6.17	−142.43	9.30	I
HBK	−25.88	27.71	−36.40	97.64	1.30	I
HER	−34.43	19.23	−43.05	85.26	0.48	I
HLP	54.61	18.82	50.80	94.87	1.12	I
HON	21.32	202.00	21.29	−88.55	12.89	I
HOP	76.51	25.01	73.54	112.62	2.30	S
HRB	47.86	18.19	43.19	93.04	0.99	I
HRN	77.00	15.37	74.48	106.20	1.87	I
HUA	−12.05	284.67	−0.81	−2.08	18.65	I
HYB	17.4	78.6	11.33	152.20	4.94	I
IQA	63.75	291.48	71.10	15.65	19.84	I
IRT	52.27	104.45	48.53	179.10	6.73	I
JAI	26.92	75.80	21.90	149.41	4.75	I
KAK	36.23	140.18	29.57	−146.21	9.04	I
KEP	−54.28	323.51	−45.91	26.07	20.53	I
KIV	50.72	30.30	46.73	104.48	1.76	I
KMH	−26.54	18.11	−37.34	87.75	0.64	I
KNY	31.42	130.88	25.17	−155.16	8.45	I
KOU	5.21	307.27	6.81	22.78	20.31	I

Table A1
Continued

IAGA code	Lat (°N)	Long (°E)	QDLat (°N)	QDLong (°E)	MLT (hr)	Source
LYC	64.60	23.75	61.50	102.51	1.63	I
LZH	36.10	103.84	31.61	177.93	6.65	I
LRM	−22.22	114.10	−32.21	−173.06	7.26	I
MAW	−67.60	62.88	−70.58	92.41	0.95	I
MCQ	−54.50	158.95	−64.10	−110.68	11.41	I
MGD	60.05	150.73	54.56	−138.48	9.56	I
MMB	43.91	144.19	37.44	−142.50	9.29	I
M08	29.44	261.39	38.67	−28.17	16.91	S
NAL	78.92	11.95	76.54	107.11	1.93	S
NOR	71.09	25.79	68.11	107.97	1.99	S
NUR	60.51	24.66	57.18	101.68	1.57	I
OTT	45.40	284.45	54.32	3.59	19.03	I
PAG	42.50	24.20	37.35	97.96	1.32	I
PBK	70.10	170.90	66.04	−126.90	10.33	S
PET	52.97	158.25	46.93	−131.25	10.04	I
PHU	21.03	105.95	15.48	179.42	6.75	I
PST	−51.70	302.11	−39.81	11.17	19.54	I
RES	74.69	265.11	82.08	−31.15	16.72	I
RPB	66.50	273.80	74.95	−12.00	17.99	S
SBL	43.93	299.99	49.42	23.24	20.34	I
SJG	18.11	293.85	25.41	12.23	19.61	I
SPG	60.54	29.72	57.18	106.15	1.87	I
SOD	67.37	26.63	64.30	106.32	1.88	I
SOL	61.08	4.84	58.33	85.18	0.47	S
STJ	47.60	307.32	51.36	31.73	20.91	I
SUA	44.68	26.25	39.92	100.02	1.46	I
TAM	22.79	5.53	12.71	80.69	0.17	I
TDC	−37.07	347.69	−41.59	50.50	22.16	I
THL	77.47	290.77	83.78	26.17	20.54	I
TRW	−43.30	294.70	−31.27	5.46	19.16	I
T15	46.24	275.66	55.92	−8.90	18.20	S
T29	58.30	291.80	65.80	14.96	19.79	S
T44	58.47	281.95	67.15	0.83	18.85	S
T47	62.20	284.35	70.44	4.83	19.11	S
T52	53.79	282.38	62.66	1.17	18.87	S
UPS	59.90	17.35	56.62	95.16	1.14	I
VOS	−78.46	106.83	−83.85	55.42	22.49	I

Data Availability Statement

Magnetic data used are part of the worldwide network of observatories INTERMAGNET (http://www.intermagnet.org/) and of the worldwide network SuperMAG (http://supermag.jhuapl.edu).

Acknowledgments
The authors kindly acknowledge V. Papitashvili and J. King at the National Space Science Data Center of the Goddard Space Flight Center for the use permission of 1 min OMNI data and the NASA CDAWeb team for making these data available (https://cdaweb.gsfc.nasa.gov/index.html/). The results presented in this paper rely on data collected at magnetic observatories. We thank the national institutes that support them and INTERMAGNET for promoting high standards of magnetic observatory practice (www.intermagnet.org). We gratefully acknowledge the SuperMAG collaborators (http://supermag.jhuapl.edu/info/?page=acknowledgement). http://sdnet.thayer.dartmouth.edu/models/dynamicmodel.php. This work is part of the PhD Thesis of L. Santarelli, who acknowledges the Dip. Scienze Fisiche e Chimiche, Università degli Studi dell'Aquila (L'Aquila, Italy). The authors acknowledge financial support from Italian PNRA under contract PNRA18_00289-A "Space weather in Polar Ionosphere: the Role of Turbulence."

References

Ahn, B.-H., Akasofu, S.-I., & Kamide, Y. (1983). The Joule heat production rate and the particle energy injection rate as a function of the geomagnetic indices AE and AL. *Journal of Geophysical Research*, *88*, 6275. https://doi.org/10.1029/ja088ia08p06275

Alberti, T., Consolini, G., Lepreti, F., Laurenza, M., Vecchio, A., & Carbone, V. (2017). Timescale separation in the solar wind-magnetosphere coupling during St. Patrick's Day storms in 2013 and 2015. *Journal of Geophysical Research: Space Physics*, *122*, 4266–4283. https://doi.org/10.1002/2016ja023175

Alberti, T., Piersanti, M., Vecchio, A., De Michelis, P., Lepreti, F., Carbone, V., & Primavera, L. (2016). Identification of the different magnetic field contributions during a geomagnetic storm in magnetospheric and ground observations. *Annales Geophysicae*, *34*, 1069–1084. https://doi.org/10.5194/angeo-34-1069-2016

Angelopoulos, V., Mukai, T., & Kokubun, S. (1999). Evidence for intermittency in Earth's plasma sheet and implications for self-organized criticality. *Physics of Plasmas*, *6*, 4161–4168. https://doi.org/10.1063/1.873681

Baker, D. N., Klimas, A. J., & Vassiliadis, D. V. (1995). Energy transfer between the solar wind and the magnetosphere-ionosphere system. *Journal of Geomagnetism and Geoelectricity*, *47*, 1171–1182. https://doi.org/10.5636/jgg.47.1171

Baker, K. B., & Wing, S. (1989). A new magnetic coordinate system for conjugate studies at high latitudes. *Journal of Geophysical Research*, *94*, 9139–9143. https://doi.org/10.1029/ja094ia07p09139

Bargatze, L. F., Baker, D. N., McPherron, R. L., & Hones, E. W. (1985). Magnetospheric impulse response for many levels of geomagnetic activity. *Journal of Geophysical Research*, *90*, 6387–6399. https://doi.org/10.1029/ja090ia07p06387

Borovsky, J. E., Elphic, R. C., Funsten, H. O., & Thomsen, M. F. (1997). The Earth's plasma sheet as a laboratory for flow turbulence in high-β MHD. *Journal of Plasma Physics*, *57*, 1–34. https://doi.org/10.1017/s0022377896005259

Consolini, G. (1997). Sandpile cellular automata and the magnetospheric dynamics. In S. Aiello (Ed.), *Proceedings of VIII GIFCO Conference. Cosmic physics in the year 2000* (p. 123). SIF.

Consolini, G. (2002). Self-organized criticality: A new paradigm for the magnetotail dynamics. *Fractals*, *10*, 275–283. https://doi.org/10.1142/s0218348x02001397

Consolini, G., & Chang, T. (2001). Magnetic field topology and criticality in geotail dynamics: Relevance to substorm phenomena. *Space Science Reviews*, *95*, 301. https://doi.org/10.1023/a:1005252807049

Consolini, G., & De Michelis, P. (2005). Local intermittency measure analysis of AE index: The directly driven and unloading component. *Geophysical Research Letters*, *32*(5), L05101. http://dx.doi.org/10.1029/2004gl022063

Consolini, G., De Michelis, P., & Tozzi, R. (2008). On the Earth's magnetospheric dynamics: Nonequilibrium evolution and the fluctuation theorem. *Journal of Geophysical Research*, *113*, A08222. https://doi.org/10.1029/2008ja013074

Consolini, G., Marcucci, M. F., & Candidi, M. (1996). Multifractal structure of auroral electrojet index data. *Physical Review Letters*, *76*, 4082–4085. https://doi.org/10.1103/physrevlett.76.4082

Cousins, E. D. P., & Shepherd, S. G. (2010). A dynamical model of high-latitude convection derived from SuperDARN plasma drift measurements. *Journal of Geophysical Research*, *115*, A12329. https://doi.org/10.1029/2010ja016017

Davis, T. N., & Sugiura, M. (1966). Auroral electrojet activity indexAEand its universal time variations. *Journal of Geophysical Research*, *71*(3), 785–801. https://doi.org/10.1029/jz071i003p00785

De Michelis, P., Consolini, G., & Tozzi, R. (2012). On the multi-scale nature of large geomagnetic storms: an empirical mode decomposition analysis. *Nonlinear Processes in Geophysics*, *19*, 667–673. https://doi.org/10.5194/npg-19-667-2012

De Michelis, P., Tozzi, R., & Consolini, G. (2013). On the nonstationarity of the decadal periodicities of the length of day. *Nonlinear Processes in Geophysics*, *20*, 1127–1135. https://doi.org/10.5194/npg-20-1127-2013

Emmert, J. T., Richmond, A. D., & Drob, D. P. (2010). A computationally compact representation of Magnetic-Apex and Quasi-Dipole coordinates with smooth base vectors. *Journal of Geophysical Research*, *115*. https://doi.org/10.1029/2010ja015326

Feldstein, Y. I., Popov, V. A., Cumnock, J. A., Prigancova, A., Blomberg, L. G., Kozyra, J. U., et al. (2006). Auroral electrojets and boundaries of plasma domains in the magnetosphere during magnetically disturbed intervals. *Annales Geophysicae*, *24*, 2243–2276. https://doi.org/10.5194/angeo-24-2243-2006

Flandrin, P., Rilling, G., & Goncalves, P. (2004). Empirical mode decomposition as a filter bank. *IEEE Signal Processing Letters*, *11*, 112–114. https://doi.org/10.1109/lsp.2003.821662

Frühauff, D., Glassmeier, K.-H., Lockwood, M., & Heyner, D. (2015). Extracting planetary waves from geomagnetic time series using empirical mode decomposition. *Journal of Atmospheric and Solar-Terrestrial Physics*, *129*, 6–12. https://doi.org/10.1016/j.jastp.2015.04.002

Gjerloev, J. W. (2012). The SuperMAG data processing technique. *Journal of Geophysical Research*, *117*. https://doi.org/10.1029/2012ja017683

Gloersen, P., & Huang, N. E. (1999). In search of an elusive Antarctic circumpolar wave in sea ice extents: 1978-1996. *Polar Research*, *18*, 167–173. https://doi.org/10.3402/polar.v18i2.6570

Hu, C. C., Miau, J. J., & Chou, J. H. (2002). Instantaneous vortex-shedding behavior in periodically varying flow. *Proceedings of the Royal Society of London A*, *458*, 911–932. https://doi.org/10.1098/rspa.2001.0898

Huang, N. E., Long, S. R., & Shen, Z. (1996). The mechanism for frequency downshift in nonlinear wave evolution. *Advances in Applied Mechanics*, *32*, 59–117. https://doi.org/10.1016/s0065-2156(08)70076-0

Huang, N. E., Shen, Z., & Long, S. R. (1999). A new view of nonlinear water waves: The Hilbert Spectrum. *Annual Review of Fluid Mechanics*, *31*, 417–457. https://doi.org/10.1146/annurev.fluid.31.1.417

Huang, N. E., Shen, Z., Long, S. R., Wu, M. C., Shih, H. H., Zheng, Q., et al. (1998). The empirical mode decomposition and the Hilbert spectrum for nonlinear and non-stationary time series analysis. *Proceedings of the Royal Society of London A*, *454*, 903–995. https://doi.org/10.1098/rspa.1998.0193

Huang, N. E., & Wu, Z. (2008). A review on Hilbert-Huang transform: Method and its applications to geophysical studies. *Reviews of Geophysics*, *46*, RG2006. https://doi.org/10.1029/2007rg000228

Iyemori, T., & Rao, D. R. K. (1996). Decay of the Dst field of geomagnetic disturbance after substorm onset and its implication to storm-substorm relation. *Annales Geophysicae*, *14*, 608–618. https://doi.org/10.1007/s00585-996-0608-3

Kamide, Y., & Kokubun, S. (1996). Two-component auroral electrojet: Importance for substorm studies. *Journal of Geophysical Research*, *101*, 13027–13046. https://doi.org/10.1029/96ja00142

Klimas, A. J., Vassiliadis, D., Baker, D. N., & Roberts, D. A. (1996). The organized nonlinear dynamics of the magnetosphere. *Journal of Geophysical Research*, *101*, 13089–13113. https://doi.org/10.1029/96ja00563

Laundal, K. M., Cnossen, I., Milan, S. E., Haaland, S. E., Coxon, J., Pedatella, N. M., et al. (2016). North-South Asymmetries in Earth's Magnetic Field. *Space Science Reviews*, *206*, 225–257. https://doi.org/10.1007/s11214-016-0273-0

Loh, C., Wu, T. C., & Huang, N. E. (2001). Application of the empirical mode decomposition-Hilbert spectrum method to identify near-fault ground-motion characteristics and structural responses. *Bulletin of the Seismological Society of America*, *91*, 1339–1357.

Lui, A. T. Y., Liou, K., Newell, P. T., Meng, C.-I., Ohtani, S.-I., Ogino, T., et al. (1998). Plasma and magnetic flux transport associated with auroral breakups. *Geophysical Research Letters*, *25*, 4059–4062. https://doi.org/10.1029/1998gl900022

McPherron, R. L., Russell, C. T., & Aubry, M. P. (1973). Satellite studies of magnetospheric substorms on August 15, 1968: 9. Phenomenological model for substorms. *Journal of Geophysical Research*, *78*, 3131–3149. https://doi.org/10.1029/ja078i016p03131

Michelis, P. D., & Consolini, G. (2015). On the local Hurst exponent of geomagnetic field fluctuations: Spatial distribution for different geomagnetic activity levels. *Journal of Geophysical Research: Space Physics*, *120*, 2691–2701. https://doi.org/10.1002/2014ja020685

Ngwira, C. M., & Pulkkinen, A. A. (2019). An introduction to geomagnetically induced currents. In J. L. Gannon, A. Swidinsky, & Z. Xu (Eds.), *Geomagnetically induced currents from the sun to the power grid, Geophysical Monograph 244* (pp. 3–12).

Pallocchia, G., Amata, E., Consolini, G., Marcucci, M. F., & Bertello, I. (2007). AE index forecast at different time scales through an ANN algorithm based on L1 IMF and plasma measurements. *Journal of Atmospheric and Solar-Terrestrial Physics*, *70*, 663–668.

Pulkkinen, A., Kuznetsova, M., Ridley, A., Raeder, J., Vapirev, A., Weimer, D., et al. (2011). Geospace Environment Modeling 2008-2009 Challenge: Ground magnetic field perturbations, *Space Weather*, *9*, S02004. https://doi.org/10.1029/2010SW000600

Richmond, A. D. (1995). Ionospheric electrodynamics using magnetic apex coordinates. *Journal of Geomagnetism and Geoelectricity*, *47*, 191–212. https://doi.org/10.5636/jgg.47.191

Roberts, P. H., Yu, Z. J., & Russell, C. T. (2007). On the 60-year signal from the core. *Geophysical & Astrophysical Fluid Dynamics*, *101*, 11–35. https://doi.org/10.1080/03091920601083820

Sharma, A. S., Sitnov, M. I., & Papadopoulos, K. (2001). Substorms as nonequilibrium transitions of the magnetosphere. *Journal of Atmospheric and Solar-Terrestrial Physics*, *63*, 1399–1406. https://doi.org/10.1016/s1364-6826(00)00241-8

Sitnov, M. I., Sharma, A. S., Papadopoulos, K., & Vassiliadis, D. (2001). Modeling substorm dynamics of the magnetosphere: from self-organization and self-organized criticality to nonequilibrium phase transitions. *Physical Review E*, *65*, 16116. https://doi.org/10.1103/physreve.65.016116

Sitnov, M. I., Sharma, A. S., Papadopoulos, K., Vassiliadis, D., Valdivia, J. A., Klimas, A. J., & Baker, D. N. (2000). Phase transition-like behavior of the magnetosphere during substorms. *Journal of Geophysical Research*, *105*, 12955–12974. https://doi.org/10.1029/1999ja000279

Tamao, T. (1986). Direct contribution of oblique field-aligned currents to ground magnetic fields. *Journal of Geophysical Research*, *91*(A1), 183–189. https://doi.org/10.1029/ja091ia01p00183

Tsurutani, B. T., Sugiura, M., Iyemori, T., Goldstein, B. E., Gonzalez, W. D., Akasofu, S. I., & Smith, E. J. (1990). The nonlinear response of AE to the IMF BSdriver: A spectral break at 5 hours. *Geophysical Research Letters*, *17*, 279–282. https://doi.org/10.1029/gl017i003p00279

Uritsky, V. M., Klimas, A. J., & Vassiliadis, D. (2001). Comparative study of dynamical critical scaling in the auroral electrojet index versus solar wind fluctuations. *Geophysical Research Letters*, *28*(19), 3809–3812. https://doi.org/10.1029/2001gl013026

Uritsky, V. M., Klimas, A. J., Vassiliadis, D., Chua, D., & Parks, G. (2002). Scale-free statistics of spatiotemporal auroral emissions as depicted by POLAR UVI images: Dynamics magnetosphere is an avalanching system. *Journal of Geophysical Research*, *107*(A12), SMP71–SMP711. https://doi.org/10.1029/2001ja000281

Uritsky, V. M., & Pudovkin, M. I. (1998). Low frequency 1/f-like fluctuations of the AE-index as a possible manifestation of self-organized criticality in the magnetosphere. *Annales Geophysicae*, *16*, 1580–1588. https://doi.org/10.1007/s00585-998-1580-x

Vassiliadis, D. V., Sharma, A. S., Eastman, T. E., & Papadopoulos, K. (1990). Low-dimensional chaos in magnetospheric activity from AE time series. *Geophysical Research Letters*, *17*, 1841–1844. https://doi.org/10.1029/gl017i011p01841

Weimer, D. R. (2013). An empirical model of ground-level geomagnetic perturbations. *Space Weather*, *11*, 107–120. https://doi.org/10.1002/swe.20030

Weimer, D. R. (2019). Empirical modeling of the geomagnetic field for GIC predictions. In J. L. Gannon, A. Swidinsky, & Z. Xu (Eds.), *Geomagnetically induced currents from the sun to the power grid, Geophysical Monograph 244* (pp. 67–78). https://doi.org/10.1002/9781119434412.ch4

Welling, D. (2019). Magnetohydrodynamic models of B and their use in GIC estimates. In J. L. Gannon, A. Swidinsky, & Z. Xu (Eds.), *Geomagnetically induced currents from the sun to the power grid, Geophysical Monograph 244* (pp. 43–65). https://doi.org/10.1002/9781119434412.ch3

Zimbardo, G., Greco, A., Sorriso-Valvo, L., Perri, S., Vörös, Z., Aburjania, G., et al. (2010). Magnetic turbulence in the geospace environment. *Space Science Reviews*, *156*, 89–134. https://doi.org/10.1007/s11214-010-9692-5